Journal of Nuclear Materials 620 (2026) 156307

Contents lists available at ScienceDirect

Journal of Nuclear Materials

journal homepage: www.elsevier.com/locate/jnucmat

Performance of high-Cr ODS steels under high-temperature neutron irradiation

Viacheslav Kuksenko [a,*], Alexandra C. Dickinson-Lomas [a], Murthy Kolluri [b], Tjark van Staveren [b], Amy S. Gandy [a]

[a] UK Atomic Energy Authority, Culham, UK
[b] NRG PALLAS, Petten, the Netherlands

ARTICLE INFO

Keywords:
Oxide dispersion strengthened steels
Ferritic ODS steels
Neutron irradiation
Atom probe tomography
Transmission electron microscopy
Precipitation
Mechanical properties

ABSTRACT

Two ferritic Oxide Dispersion Strengthened (ODS) steels Fe-12Cr-YWT and Fe-14Cr-YWT were irradiated in the High Flux Reactor (HFR) to an approximate dose of 3 dpa at a nominal temperature of 600 °C. Tensile tests at room and elevated temperatures as well as microstructural investigations using transmission electron microscopy (TEM) and atom probe tomography (APT) were performed to study evolution of the ODS steels during the high-temperature neutron exposure. Both steels had similar responses to the neutron irradiation in HFR. Tensile testing demonstrated very little effect of irradiation on strength and plasticity. Scanning transmission electron microscopy (STEM) studies showed stable fine distribution of Ti-Y oxides before and after irradiation, with larger sized precipitates at grain boundaries (10–30 nm) and smaller precipitates within the matrix (<10 nm). APT measurements confirmed high stability of Y-based oxides with relatively small increase of the average diameter (about 20 %) after irradiation and stable number density of the clusters. STEM-Energy Dispersive X-ray (EDX) analysis revealed the presence of W-rich Laves phase precipitates at grain boundaries (GBs) in both steels after neutron exposure in HFR. In both steels, a 50 % drop in matrix W content was measured by APT, consistent with the STEM observations of W-rich Laves phases at GBs. Finally, an increase in number density of Cr rich carbides was observed in the Fe-12Cr-YWT steel after irradiation.

1. Introduction

Developing advanced structural materials is crucial for realizing future commercial fusion energy. Components in the breeder blanket coolant outlet region may need to operate between 600 and 700 °C. However, conventional reduced activation ferritic-martensitic (RAFM) steels like F82H or EUROFER97 are limited to an upper temperature boundary of < 550 °C [1] or, for some novel advanced RAFM steels with lower technological maturity [2], up to 600 °C. Oxide Dispersion Strengthened (ODS) steels development was largely driven by the fact that the traditional process manufactured ferritic-martensitic (FM) steels do not possess adequate mechanical properties at temperatures of 600–700 °C [3]. ODS steels are characterized by highly dispersed nano-sized, highly thermally stable oxide particles with sizes ranging from 1 to 20 nm and distribution densities ranging from 10^{22} to 10^{24} m^{-3}. Oxide particles inhibit grain-boundary and dislocation motion, improving high temperature strength and creep resistance [3]. Therefore, it is expected that the presence of nano-oxide particles will enable ODS ferritic and ferritic-martensitic steels to meet the harsh operating conditions in fusion [4–7] and advanced fission reactors [7–11].

The presence of nano-dispersed precipitates can significantly improve irradiation damage resistance of steels, by acting as free surfaces for recombination of neutron irradiation induced defects and by trapping transmutant helium, produced during fusion neutron irradiation [12]. For example, it was experimentally demonstrated that the presence of nano-scale Y_2O_3-particles in EUROFER97 steel provided increased resistance to radiation induced embrittlement: tensile tests of HFR neutron irradiated EUROFER97 samples (T_{irr}=250 °C and 350 °C, 16.3 dpa) showed high strain localisation and almost complete loss of the uniform elongation, however this was not observed in the ODS EUROFER97 steel which contained nano-scale Y_2O_3-particles [13].

It is known that segregation of solutes and the formation of new phases can affect mechanical and corrosion properties of structural

* Corresponding author.
E-mail address: slava.kuksenko@ukaea.uk (V. Kuksenko).

https://doi.org/10.1016/j.jnucmat.2025.156307
Received 28 September 2025; Received in revised form 13 November 2025; Accepted 13 November 2025
Available online 14 November 2025

steels [1] and a fundamental understanding of the role of material chemistry and microstructural constituents on radiation damage resistance is the driving force for numerous studies on Fe-Cr based steels including ODS steels. Chromium content has been shown to be among the key parameters to optimize their properties under irradiation. For example, significant irradiation induced hardening was observed in high-chromium (Cr > 12 wt %) ODS steel, irradiated in ORNL's High Flux Isotope Reactor (HFIR) at 400 °C–500 °C, up to a maximum dose of 23.3 dpa [14]. Such behaviour is expected to be linked to the formation of the radiation-enhanced Cr-rich alpha-prime phase typically observed in steels with Cr content above 8–9 wt % [14]. Formation of a large variety of other secondary phases has been also reported in irradiated Fe-Cr based steels including Cr, Si and Ni enriched M_6X precipitates [15–17], Cr and V enriched M_2X precipitates [16,18,19]; Ni and Si enriched G- [16,20], χ (Chi)- [15–18,21] and σ (sigma)- phases [15,22], MP and M_3P type phosphides [15], and W-rich [23,24] Laves phases. Despite being known to affect mechanical and corrosion properties of Fe-Cr based steels [1], these secondary phases are given very little attention in available ODS steel literature.

One of the critical challenges when developing ODS steels for nuclear applications is understanding the effects of neutron irradiation on microstructural stability of the strengthening nano-sized oxides. There are observations of structural evolution and chemical changes occurring in nano-oxides during irradiation (see reviews [25,26] and references cited) but there is no clear correlation between the evolution of oxide size and number density changes, dose and irradiation temperature. In general, data on performance of ODS steels under irradiation are still substantially limited compared to RAFM steels. A fundamental understanding of the effect of oxide particle evolution combined with the effects of phase stability on ODS steels' thermo-mechanical properties is needed. ExtreMat-I and ExtreMat-II neutron irradiation campaigns in the HFR (NRG PALLAS, Petten) have been designed by the cross-disciplinary extreme environments materials community with the aim to develop radiation resistant materials for aggressive high heat flux applications under very intense irradiation [27]. The main efforts have been focused on materials with operational temperatures well above 600 °C including ferritic ODS steels. For the first time this manuscript reports the effects of the ExtreMat-II neutron irradiation on mechanical properties of two Fe-12Cr-YWT and Fe-14Cr-YWT based ODS steels in combination with detailed pre- and post-irradiation microstructural studies. Both steels were irradiated at a target temperature of 600 °C with Fe-12Cr-YWT irradiated to a fluence ($E > 1$ MeV), of 2.16×10^{25} m^{-2} and Fe-14Cr-YWT to a fluence of 1.71×10^{25} m^{-2}, with the equivalent displacement doses of 3.14 dpa and 2.51 dpa, respectively. This work contributes to filling the current knowledge gap in understanding the complex response of ODS alloys to high temperature neutron radiation in terms of mechanical properties performance and microstructural evolution.

2. Material and techniques

2.1. Material

Two ferritic ODS steels Fe-12Cr-YWT and Fe-14Cr-YWT are investigated in this work, and their chemical compositions reported in Table 1. The steels were fabricated by mechanical alloying Fe, Cr, W and Ti elemental powders with 0.3wt % of Y_2O_3 powder particles followed by Hot Isostatic Pressing (HIP) at the Plasma Physics Research Centre, EPFL (Switzerland). The details of the fabrication process of these steels is given in papers [28–30].

2.2. EXTREMAT -II irradiation

The irradiation was carried out in leg 4 of a QUATTRO rig, positioned at C7 in the HFR (Fig. 1). The irradiation lasted for eight reactor cycles, corresponding to a total of 208 full-power days (FPDs). The samples

Table 1
Nominal chemical composition of the examined ODS steels [28].

Element	Fe-12Cr-YWT		Fe-14Cr-YWT	
	wt %	at %	wt %	at %
Cr	11.8	12.5	13.7	14.5
Mn	0.12	0.12	0.16	0.16
Si	0.028	0.06	0.031	0.06
C	0.086	0.4	0.088	0.4
N	0.033	0.13	0.035	0.14
O	0.47	1.6	0.48	1.6
Ti	0.25	0.29	0.26	0.3
Y	0.25	0.16	0.23	0.14
Mo	0.007	0.004	0.008	0.004
W	1.86	0.56	1.84	0.55
Fe	Balance	Balance	Balance	Balance

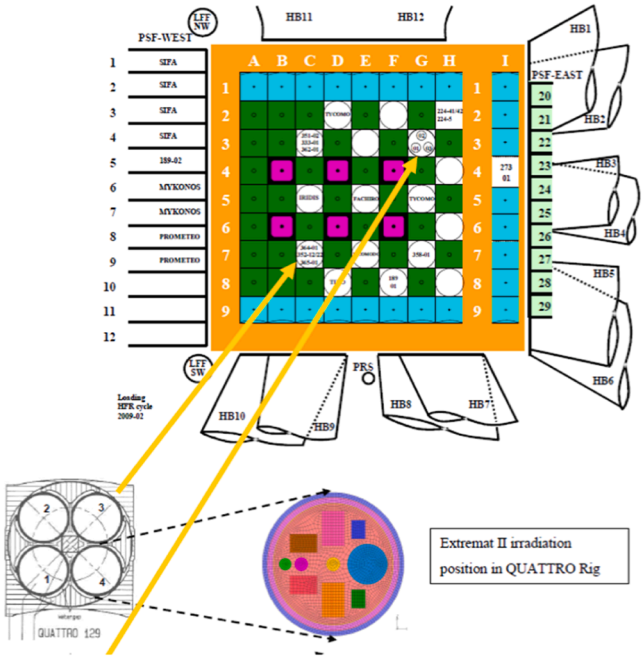

Fig. 1. Schematic representation of the location Extremat-II capsule in the HFR. The irradiation was carried out in leg 4 of a QUATTRO rig, positioned at C7.

were irradiated in an inert gas atmosphere consisting of a helium–neon mixture. A drum-based design was employed, in which the samples were inserted into TZM drums. These drums, containing the samples, were placed inside a stainless-steel sample holder tube, which was then positioned within the irradiation rig tube in leg 4 of the QUATTRO rig. The target temperature was achieved by tailoring the gas gaps between (i) the drums and the sample holder tube, and (ii) the outer stainless steel sample holder tube and the irradiation rig tube, as well as by adjusting the helium - neon gas composition.

Fe-12Cr-YWT and Fe-14Cr-YWT ODS steels were irradiated at a target temperature of 600 °C to fluences ($E > 1$ MeV) of $2.16\times10^{25}m^{-2}$ (3.14 dpa) and $1.71\times10^{25}m^{-2}$ (2.51 dpa), respectively [31]. The nominal fluence rate values are 9.51×10^{17} n/(m^2s) for Fe-12Cr-YWT and 1.20×10^{18} n/(m^2s) for Fe-14Cr-YWT.

The target temperature was achieved by tailoring the gas gaps between (i) the drums and the sample holder tube, and (ii) the outer stainless steel sample holder tube and the irradiation rig tube, as well as by adjusting the helium - neon gas composition. The dpa values reported are dpa in steel calculated by convoluting the neutron spectrum averaged over the drum in the sample holder (calculated using MCNP) with the dpa cross-sections from the DAMSIG-2001 library. The DAMSIG-

2001 data comes from the file DAMS2005.LIB.

The details of the HFR irradiation parameters are summarised in Table 2. For the sake of simplicity, the irradiation conditions throughout this manuscript will be referred to as 600 °C and 3 dpa

2.3. Mechanical testing

The tensile tests have been performed at NRG PALLAS on Instron electro-mechanical machines. The testing assembly is equipped with a 10 kN dynamic load cell and a three-zone furnace. The furnace temperature is controlled by temperature controllers to within ±2 °C. Before a test series is started, the furnace is routinely verified with thermocouples at different locations on the specimen.

The tensile tests were performed between room temperature (RT) and 600 °C, specifically at RT, 150, 300, 400, 500, 550, and 600 °C. One tensile test was conducted at each temperature, except for the as-received Fe-12Cr-WTY alloy at 550 °C, for which two data points will be reported. Flat mini tensile specimens of external dimension 25.5 × 5 × 0.25 mm were used. All tests were performed in accordance with ASTM E8M [32], except that the crosshead displacement sensor was used and the elastic reaction of the entire load strain was measured. The strains reported are therefore all plastic strains, offset to a fitting of the elastic slope.

The tensile tests were performed with a constant actuator velocity, resulting in an initial strain rate of 5×10^{-4} s^{-1}. From the load-displacement curves, strength data at specific plastic strain intervals were calculated. The 0.2 % offset Yield Stress (YS), the Ultimate Tensile Strength (UTS), plastic Uniform Elongation (UE), and Total Elongation (TE) are presented here. Both the total elongation and uniform elongation used and presented in this manuscript are derived from the load-displacement curves .

2.4. Analysis of microstructure with scanning electron microscopy

Before microstructural investigation, the surfaces of the samples were mechanically ground and polished with SiC paper, diamond paste and finished with 0.05 μm alumina suspension. To investigate the grain structure and crystallography of the samples, EBSD analyses were performed, using the UKAEA TESCAN Mira3 XMH scanning electron microscope (SEM) equipped with a high brightness Field Emission Gun and Oxford Instruments Symmetry 2 EBSD detector. The step size for the EBSD data collection was between 10 and 65 nm depending on the scanned area and required resolution. Aztec Crystal software was used for analysis of the EBSD data following the gridline method in ASTM E2627 [33].

2.5. Analysis of microstructure with TEM

TEM specimens were produced from both as-received and irradiated samples using a Ga focussed ion beam Helios NanoLab 600i at the Materials Research Facility, UKAEA. Thin windows were created in each sample, and final polishing was carried out at 5 kV.

Scanning transmission electron microscopy and energy dispersive X-ray spectroscopy (STEM-EDX) have been used to examine the morphology and composition of phases present in the alloys before and after irradiation. STEM imaging and EDX mapping was carried out on FEI Talos TF200X CSTEMs with Super-X EDX detectors, at the University of Manchester (as-received specimens) and University of Birmingham (neutron-irradiated specimens). Velox™ (v2.15, ThermoFisher Scientific) was used for data acquisition and image processing, and HyperSpy v2.2.0 [34] was used to extract EDX spectra and create EDX maps for relevant elements. FIJI (ImageJ) [35] was used to analyse Laves phase precipitate distribution, by thresholding high-angled annular darkfield (HAADF) images to extract overlays of W-rich precipitates and obtain a distribution of precipitate equivalent diameters.

Table 2
Irradiation parameters for the ODS steels used in this work [31].

Material	EXTREMAT II samples position	T median, °C	T max, °C	Dose, dpa
12Cr-WTY	Drum 2	589	617	3.14
14Cr-WTY	Drum 1	601	632	2.51

2.6. Analysis of microstructure with atom probe tomography

Samples for atom probe tomography examination were prepared using the UKAEA Helios NanoLab 600i FIB system dedicated for radioactive materials. Initially a 25 μm × 7 μm foil, 2 μm in thickness, was produced from the irradiated sample. Then 2 μm × 2 μm × 7 μm columns were cut from the foil and one-by-one welded by Pt deposition to pre-tips (stainless steel needles). Annular milling was used to obtain sharp tips suitable for APT analysis.

The samples were studied using the laser assisted tomographic atom probe LEAP 5000 XR at the University of Oxford. During experiments, the specimens were cooled to 50 K to mitigate preferential evaporation. The analyses were performed using laser pulses with an energy of 40pJ. The basic principle of the APT technique can be found in Refs. [36,37].

During this study, the following Atom Probe Tomography (APT) samples were analysed:

- Fe-12Cr-YWT:
  - As-received condition – 3 samples (130 million collected ions)
  - Irradiated condition – 3 samples (135 million collected ions) Fe-14Cr-YWT:
- As-received condition – 3 samples (20 million collected ions)
  - Irradiated condition – 3 samples (160 million collected ions)

3D images and data treatment were performed using the CAMECA IVAS software. To measure the size and the number density of clusters, a data filter in composition IVAS "Cluster Analysis" method was used. The filter enables the different phases to be distinguished owing to their chemical composition and defines clusters by setting a minimum number of ions, N_{min}, separated from each other a distance shorter than d_{max}. Y, Y-O and Ti-O ions have been used for cluster identification, using the following cluster search parameters: $d_{max} = 1$ nm, $N_{min} = 7$. Details on the cluster selection parameters in ODS steels, N_{min} and d_{max}, can be found in [38]. The cluster size was calculated as the Guinier diameter [36,37].

2.7. ThermoCalc modelling of thermal phase stability and precipitation kinetics

ThermoCalc 2024a with the TCFE12:Steels/Fe-alloys v12.0 database and the PRISMA module [39], has been used to model thermally stable phase fractions and compositions after ageing at 600 °C for 180 days, to mimic the time and target temperature of the neutron irradiation exposures. Compositions were simplified in these models, omitting impurities and modelling only Fe, Cr, O, Ti, Y, W and C. An average grain size was used corresponding to the area-weighted mean equivalent circle diameters of the microscopic grains to provide a comparison with the regions of smaller grains imaged in the TEM datasets.

3. Experimental results

3.1. Tensile properties

Fig. 2 shows (a) Yield stress, (b) ultimate tensile stress, (c) uniform elongation and (d) total elongation versus test temperature of the Fe-

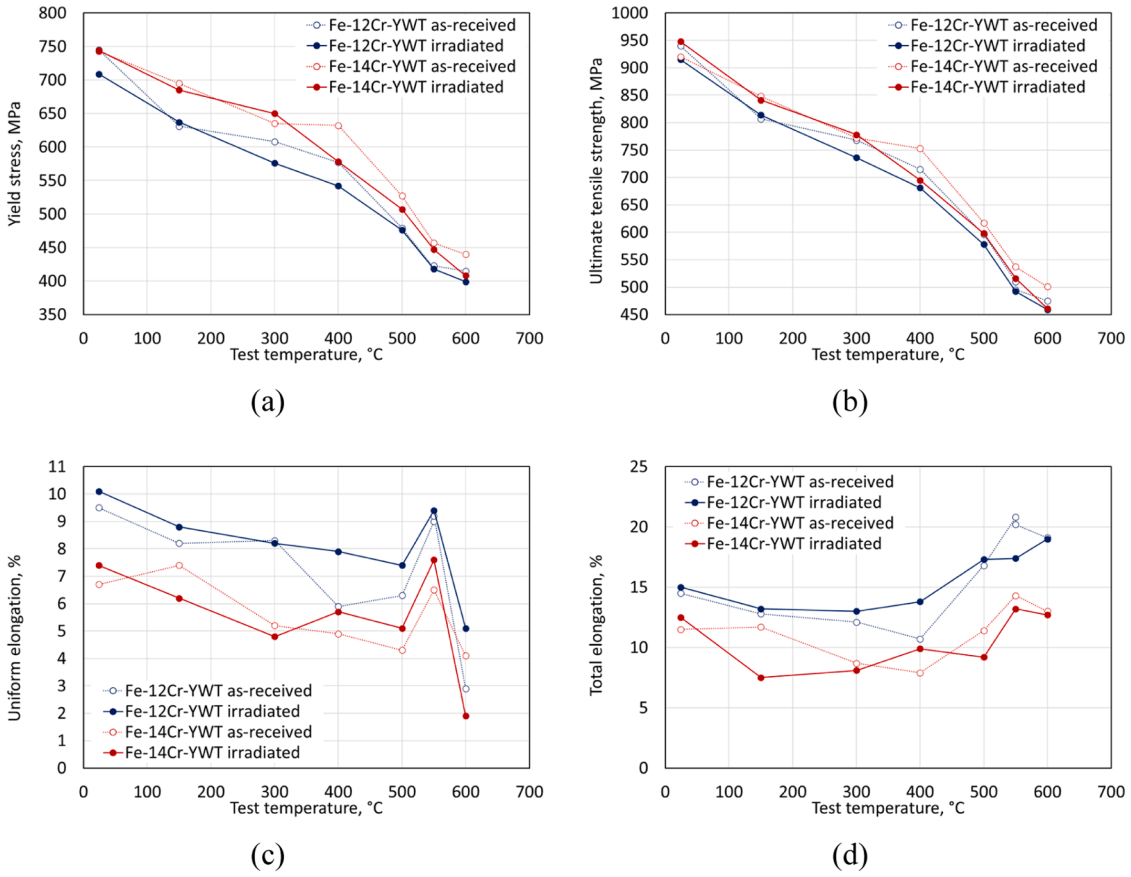

Fig. 2. (a) Yield stress, (b) ultimate tensile stress, (c) uniform elongation and (d) total elongation versus test temperature of the Fe-12Cr-YWT and Fe-14Cr-YWT ODS steels before and after neutron irradiation in HFR.

12Cr-YWT and Fe-14Cr-YWT ODS steels before and after neutron irradiation in HFR. Summary of the numerical data from the tensile tests is provided in Appendix A. Both ODS steels exhibited a high tensile strength and a reasonable ductility up to 600 °C, the maximum tensile test temperature used in this study (see Fig. 2). The Fe-14Cr-YWT ODS steel appears somewhat stronger and less ductile than the Fe-12Cr-YWT ODS steel, with a room-temperature yield strength of over 740 MPa compared with around 710 MPa for the Fe-12Cr-YWT ODS steel. The yield strength (YS) and ultimate tensile strength (UTS) of both steels decreased with increasing the test temperature (see Fig. 2(a) and (b)). Both steels exhibited a relatively monotonic decrease by about 50–65 MPa per 100 °C of test temperature, declining to about 410–440 MPa at 600 °C. Similar trends are often observed in other ODS steels [26,28,40–42]. The total plastic elongation (see Fig. 2(c)) of both steels initially decreased with test temperature, until it reached a minimum value at about 400 °C, and then increased with increasing test temperature until 550 °C, followed by a small decrease at 600 °C. The uniform elongation of both steels decreased more or less continuously with increasing test temperature (see Fig. 2(d)), but exhibited a sharp peak at about 550 °C. Oksiuta et al. [28] suggested that this phenomena might be associated with a dynamic recrystallization or a change in rate controlling slip system occurring at this temperature, however the exact mechanism is currently not identified.

These results suggest neutron irradiation leads to relatively minor changes in the tensile properties of both ODS steels. Both YS and UTS exhibit a slight decrease of about 3 % compared with the values before irradiation. Evolution of TE and UE did not show a clear trend and stayed within 5 % and 2 % (absolute in both cases), respectively, compared to the TE and UE values measured before irradiation.

3.2. Grain structure of the alloys

Fig. 3 shows the surface normal-projected inverse pole figure (IPF) orientation EBSD maps of the ODS samples: Fe-12Cr-YWT (a) and Fe-14-YWT (b), prior to irradiation. Both alloys have two distinct microstructural areas with dissimilar grain size distributions: i) micro- and ii) nanometre sized grains (Fig. 3). Micrometric grains had a size of approximately 1 to 15 μm and represented about 85 % and 70 % of the microstructure in Fe-12Cr-YWT and Fe-14Cr-YWT, respectively. The corresponding area-weighted mean equivalent circle diameters of the micrometre sized grains were 3.9 ± 1.3 um for Fe-12Cr-YWT and 3.5 ± 1.1 um for Fe-14Cr-YWT. The remaining area is occupied by nanometric grains, representing approximately 15 % and 30 % of the microstructure in Fe-12Cr-YWT and Fe-14Cr-YWT, respectively. Higher magnification EBSD studies showed that the nanometre sized grains had a size range between 100 and500 nm in both steels. Approximately 30 % of the grain boundaries in the nanometre -sized areas were low-angle grain boundaries (grain misorientation <10°). Similar bimodal grain size distributions have been reported in HIPed Fe-Cr ferritic [43–45] and martensitic [46] ODS steels. The underlying mechanism remains not fully understood. It is generally believed that incomplete recrystallization and non-uniform grain growth are the primary contributors to this bimodality [44]. Additionally, the study in [45] suggests that larger ferrite grains may form in regions with a lower density of fine-scale precipitate phases, which promotes recovery and grain growth.

3.3. Evolution of precipitates and secondary phases after irradiation

The unirradiated microstructures of Fe-12Cr-YWT and Fe-14Cr-YWT both showed fine distributions of Y-Ti-O (< 10 nm), with larger Y-Ti-O

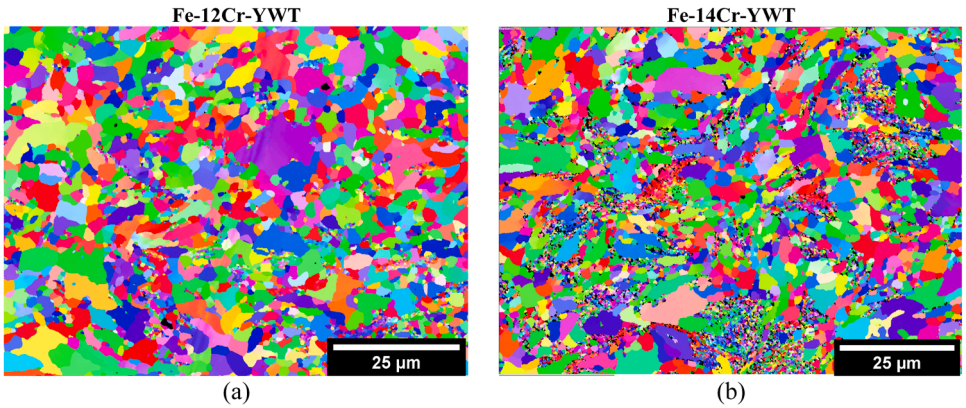

Fig. 3. Surface normal-projected inverse pole figure (IPF) orientation EBSD maps of the ODS samples: Fe-12Cr-YWT (a) and Fe-14-YWT (b). Both alloys have two distinct microstructural areas with micrometric and nanometric sized grains. The step sizes for EBSD mapping were 65 nm for the Fe-12Cr-YWT alloy and 50 nm for the Fe-14Cr-YWT alloy, respectively.

(10–30 nm) at grain boundaries (e.g., Fig. 4, showing Y-Ti-O precipitates in Fe-12Cr-YWT, indicative of both steels studied). In addition, Ti and Cr rich oxides (50–300 nm) were also found at grain boundaries, and are likely to be TiO_2 based oxides typically observed in ODS steels [5,47].

Identical matrix and grain boundary Y-Ti-O precipitates are observed by STEM in the neutron irradiated Fe-12Cr-YWT and Fe-14Cr-YWT steels, indicating high stability of this phase under neutron exposure at 600 °C (Fig. 5). Previous studies on neutron irradiated alloys at similar doses also tend to show minimal changes in nano-scale oxide dispersion, or a small amount of coarsening [48,49]. TiO_2 based precipitates at grain boundaries remained stable as well.

The most noticeable microstructural evolution detected by STEM was the formation of a new W-rich phase which appeared at grain boundaries, observed as areas of high intensity in the HAADF images in Fig. 6. EDX spectra from regions of the W rich precipitates in both alloys, Figs. 7 and 8, suggest that the main constituents of these precipitates are Fe, W and Cr, indicating an intermetallic precipitate, likely to be Fe_2W Laves phase. The Fe_2W Laves phase has been observed in a wide range of ferritic and ferritic-martensitic steels exposed to ageing and neutron irradiation at around 600 °C [50–53]. The area fraction of Laves phase precipitates has been calculated for each of the irradiated alloys by thresholding and analysing HAADF images of TEM specimens using FIJI software [35]. There is no significant difference in the area fraction between the Fe-12Cr-YWT and Fe-14Cr-YWT steels (Table 3). A smaller average size and higher number density (ND) of Laves phase precipitates was measured in the Fe-14Cr-YWT sample, but this is most likely to be due to the region of nanosized grains present in this specimen resulting in a much higher density of grain boundaries, and therefore nucleation sites, compared with the Fe-12Cr-YWT lamella. The total areas of images used for this analysis for the Fe-12Cr-YWT and Fe-14Cr-YWT were only 70.9 μm^2 and 51.9 μm^2, respectively, so are unlikely to provide representative areas given the possible inhomogeneity of these steels.

In addition, a Cr-rich carbide phase was observed at grain boundaries after irradiation (Figs. 7 and 9) in the Fe-12Cr-YWT alloy, compared with the as received specimen (Fig. 4).Various ageing studies of C containing ODS steels also reported presence of carbides [52,54,55]. These were generally observed to be co-located with Laves phase precipitates, as shown in Fig. 9. Similar observations have been made in RAFM steels,

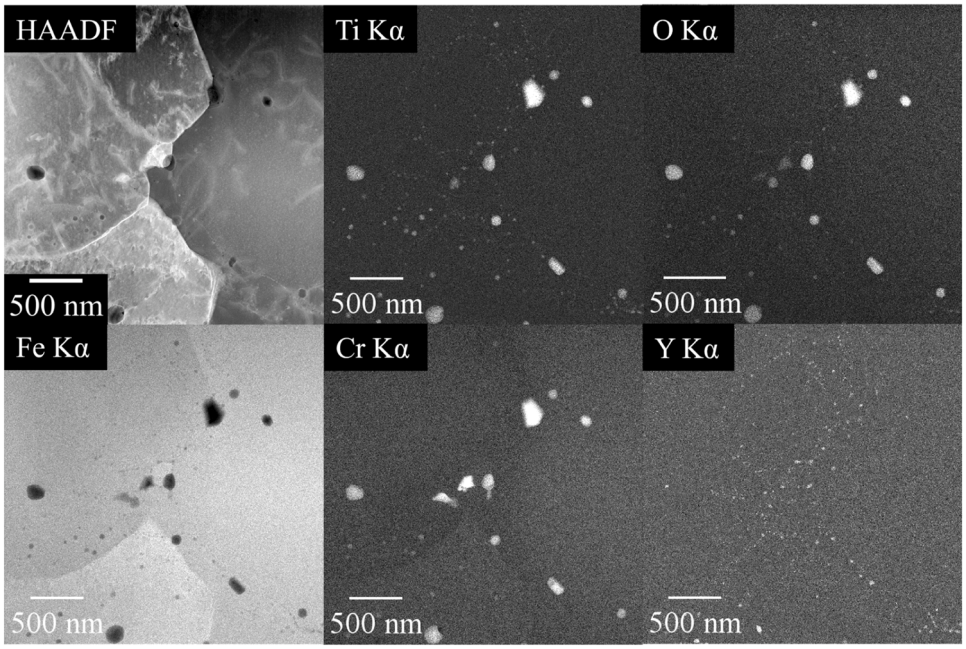

Fig. 4. HAADF STEM image, and background subtracted EDX intensity maps for Fe, Ti, Cr, O and Y Kα X-ray emissions, showing a region of unirradiated 12Cr ODS steel showing the presence of Cr-Ti oxides and finer scale Y-Ti-O oxides present throughout the material.

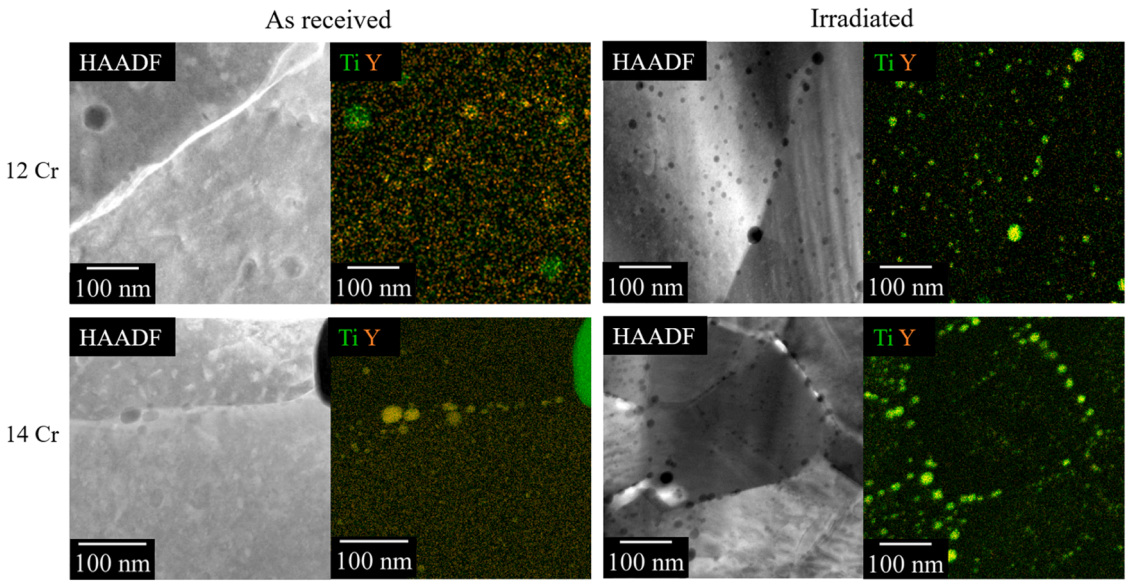

Fig. 5. High angle annular dark field (HAADF) images and Y and Ti EDX net count maps showing larger Y-Ti-O precipitates along grain boundaries, compared with finer precipitates in the ferritic matrix, in unirradiated and neutron irradiated (3 dpa, 600 °C) Fe-12Cr-YWT and Fe-14Cr-YWT steels.

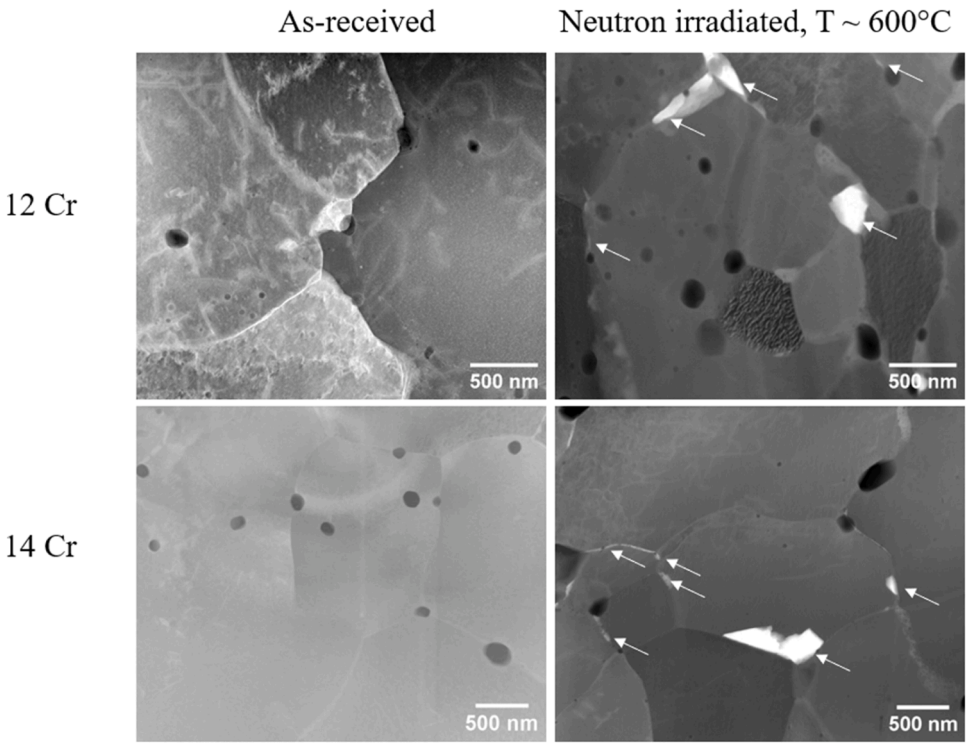

Fig. 6. HAADF images of Fe-12Cr-YWT (top) and Fe-14Cr-YWT (bottom) ODS steels, showing dark rounded precipitates of TiO_2 based oxides present in the matrix and on grain boundaries in unirradiated material (left). Images on the right-hand side show additional grain boundary precipitates with strong mass contrast (indicated by arrows), formed after neutron irradiation (3dpa, 600 °C) in the Fe-12Cr-YWT and Fe-14Cr-YWT steels.

with Laves phase nucleating both independently at interfaces, or wrapping around existing $M_{23}C_6$ carbides [51]. The EDX spectrum for the Cr-rich carbide in Fig. 9 is consistent with $M_{23}C_6$ ($Cr_{17}W_3Fe_3C_6$) carbides occasionally observed in other ODS steels, with a slight enrichment in W [54,51].

It should be noted, that after irradiation, under-over focus TEM imaging of nanoscale features did not show a change in contrast that would indicate the presence of voids and, in general, features observed in STEM images were associated with Y and Ti characteristic X-ray emissions suggesting that irradiation has not led to void formation.

3.4. Nanoscale analysis of oxide phase

Compositions of the ODS samples before and after irradiation as measured by APT are given in Tables 4 and 5. Bulk compositions are calculated by counting the total quantity of atoms of every alloying element in an entire APT volume, and the values are averaged over several datasets. Within uncertainties, the bulk compositional data from

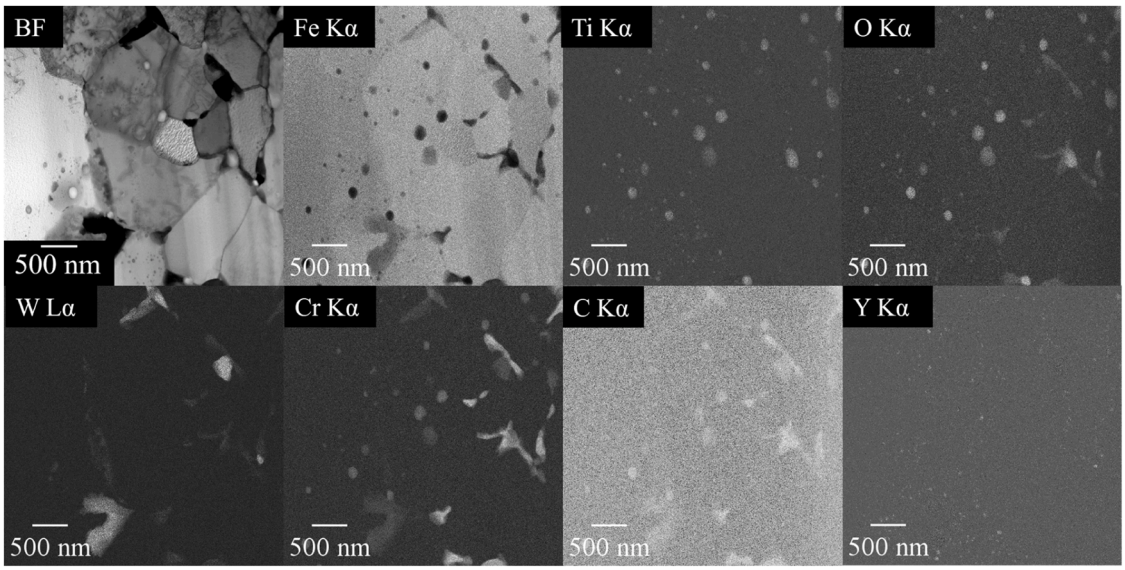

Fig. 7. Bright-field STEM image, and EDX maps for Fe, Ti, O, W, Cr, C and Y, of a region of neutron irradiated (3dpa, 600 °C) Fe-12Cr-YWT ODS steel showing the presence of Ti and Cr rich TiO_2 based oxides, finer scale Y-Ti-O oxides, as well as new Laves phase precipitates at grain boundaries.

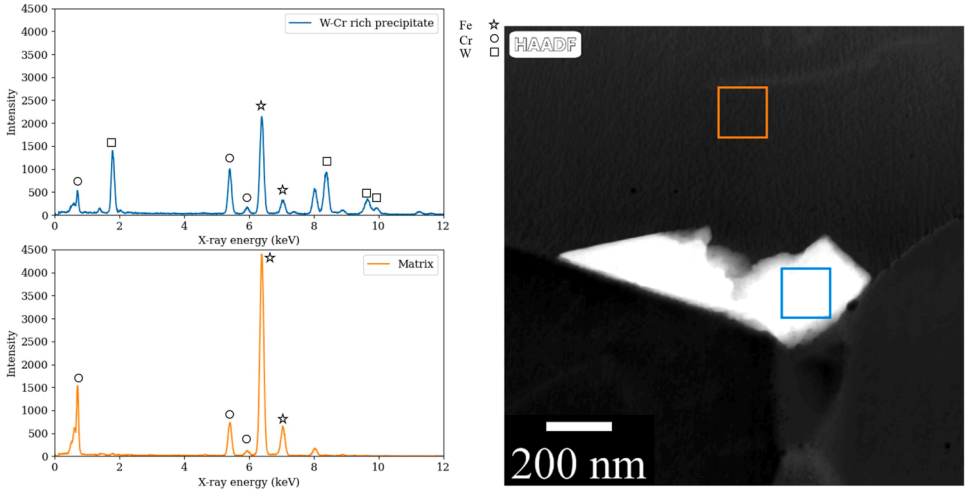

Fig. 8. EDX spectra obtained from areas of the HAADF STEM imaged region shown on the right, showing the difference in characteristic X-ray emissions from a Laves phase precipitate and the Fe-Cr matrix. 8 keV peaks originate from background TEM holder scattering from Cu.

Table 3
Area weighted average number density, equivalent diameter and area fraction of Laves phase precipitates observed in the two neutron irradiated alloys (3dpa, 600 °C) across a range of grain size regions.

Alloy	ND (m^{-2})	Average diameter (nm)	Area fraction (%)
Fe-12Cr-YWT	$6.06 \pm 0.04 \times 10^{11}$	153 ± 4	1.59 ± 0.08
Fe-14Cr-YWT	$1.75 \pm 0.08 \times 10^{12}$	106 ± 2	1.79 ± 0.03

APT are in reasonable agreement with the chemical analysis of the steels as given in Table 1 for the majority of the elements detected [28]. However, APT measured lower Mn, Si, C, N impurities content as well as half the expected oxide forming Y, Ti and O. This might originate from the chemical non-homogeneity of the material. As was demonstrated by TEM (Fig. 6), larger Y-Ti-O enriched oxides, TiO_2 oxides, and Cr carbides are located at grain boundaries with the number density too small to be analysed by APT.

The matrix compositions are calculated in a similar manner, but atoms defined as part of a cluster by the IVAS "Cluster Analysis" algorithm are excluded. It is noticeable that the oxide forming Y and Ti are present in the matrix in very small quantities (<50 appm and <200 appm correspondently).

In general, no substantial change in bulk and matrix composition measurements occur during irradiation, except for one element – W. In both steels, only about half of W is detected after irradiation. This agrees with the diffusion of W towards grain boundaries and formation of Laves phase, as was observed by our TEM examination (see Fig. 6).

APT 3D maps (Figs. 10 and 11) clearly demonstrates the presence of nanometric ODS precipitates distributed in the matrix - spherical clusters enriched by Y, Ti and O. The summary of the cluster analysis statistics is given in Table 6 and the size distribution is demonstrated in Fig. 12. Before irradiation the number density (ND) of the ODS precipitates is about 7 times larger in the Fe–14Cr-YWT than in the Fe–12Cr-YWT: 3.9×10^{23} m^{-3} vs 5.5×10^{22} m^{-3}, respectively. ODS precipitates are more homogeneously distributed in the Fe-14Cr-YWT,

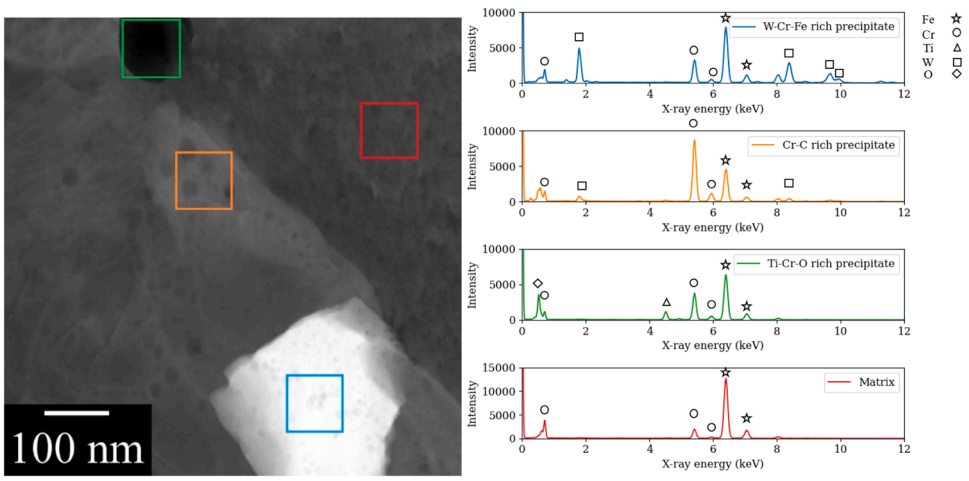

Fig. 9. EDX spectra obtained from areas of the HAADF STEM imaged region of neutron-irradiated (3dpa, 600 °C) Fe-12Cr-YWT ODS shown on the right, showing the difference in EDX spectra from the Laves phase, Cr-rich carbide, TiO_2 based oxide, and the Fe-Cr matrix.

Table 4
Compositions of the Fe-12Cr-YWT ODS samples before and after irradiation (3dpa, 600 °C) as measured by APT.

Element	Fe-12Cr-YWT			
	Bulk composition (entire data set)		Matrix composition (composition excluding precipitates)	
	Before irradiation (at %)	After irradiation (at %)	Before irradiation (at %)	After irradiation (at %)
Cr	12.2 ± 0.6	11.9 ± 0.1	12.2 ± 0.6	11.9 ± 0.1
Y	0.07±0.03	0.07±0.01	0.001 ± 0.001	0.001 ± 0.001
Ti	0.13±0.03	0.13±0.08	0.008 ± 0.001	0.011 ± 0.003
O	0.3 ± 0.1	0.3 ± 0.2	0.07±0.04	0.09±0.02
W	0.5 ± 0.1	0.25±0.01	0.5 ± 0.1	0.25±0.01
Mn	0.008±0.004	0.02±0.01	0.006±0.002	0.017±0.002
Si	0.002±0.001	0.007±0.002	0.001±0.001	0.001±0.001
C	0.002 ± 0.002	0.002 ± 0.001	0.001 ± 0.001	0.001 ± 0.001
N	0.03±0.02	0.02±0.01	0.03±0.02	0.02±0.01
P	0.001±0.001	0.001±0.001	0.006±0.002	0.001±0.001
Ar	0.002±0.002	0.002±0.001	0.002±0.002	0.002±0.002
Fe	Balance	Balance	Balance	Balance

Table 5
Compositions of the Fe-14Cr-YWT ODS samples before and after irradiation (3dpa, 600 °C) as measured by APT.

Element	Fe-14Cr-YWT			
	Bulk composition		Matrix composition	
	Before irradiation (at %)	After irradiation (at %)	Before irradiation (at %)	After irradiation (at %)
Cr	15.2 ± 1.3	14.2 ± 1.3	14.9 ± 1.2	14.3 ± 0.1
Y	0.11±0.03	0.11±0.01	0.003 ± 0.001	0.001 ± 0.001
Ti	0.13±0.05	0.13±0.01	0.02 ± 0.01	0.02 ± 0.01
O	0.4 ± 0.1	0.3 ± 0.1	0.21±0.09	0.11±0.02
W	0.57±0.09	0.27±0.01	0.57±0.09	0.27±0.01
Mn	0.011±0.001	0.011±0.001	0.009±0.002	0.019±0.002
Si	0.007±0.001	0.019±0.001	0.006±0.004	0.001±0.001
C	0.009 ± 0.005	0.004 ± 0.003	0.009 ± 0.004	0.004 ± 0.004
N	0.08±0.04	0.09±0.01	0.08±0.03	0.08±0.01
P	0.001±0.001	0.001±0.001	0.001±0.001	0.001±0.001
Ar	0.005±0.001	0.001±0.001	0.005±0.001	0.001±0.001
Fe	Balance	Balance	Balance	Balance

as demonstrated by the smaller deviation of the minimum and maximum ND from the average values (Table 6). Irradiation did not significantly change the number density of the nanosized oxides. The average diameter of the Y-Ti-O oxides is slightly larger in the Fe-12Cr-YWT (2.5 ± 1.1 nm) than in the Fe-14Cr-YWT (2.2 ± 0.5 nm). Irradiation led to an increase in the average diameter in both steels to 3.2 ± 2.2 nm in the Fe-12Cr-YWT (28 % increase) and 2.5 ± 0.7 nm in the Fe-14Cr-YWT (14 % increase). It should be noted that before and after irradiation, the diameter size distribution is broad, and the increase of the averaged diameter stays within the standard deviation. However, the size frequency distribution in Fig. 12 clearly confirms oxide growth in both ODS steels. In the irradiated steels, in addition to the small increase of the mean diameter, a noticeable broadening of the size distribution towards larger sizes is observed.

The composition of the Y-Ti-O clusters, as measured by APT for as-received and irradiated samples, is given in Tables 7 and 8. Raw composition measurements suggest an Fe concentration of between 60 and 70 at. % in the Y-Ti-O clusters. Such high Fe content is consistent with the previously reported APT measurements of nano-oxides in different ferritic and ferritic-martensitic ODS steels [56–58]. While it is possible that the oxides may contain some iron, it is generally considered that such very high levels are mainly the result of trajectory aberrations, an APT artifact known to occur with small precipitates [37,59]. Following the approach suggested in [56], the quantity of Fe in Y-Ti-O oxides was set to zero and the matrix contribution was estimated by calculating the proportion of other elements present in the matrix (Cr, W, etc.) to Fe and removing this number of atoms from the raw cluster composition. Matrix-corrected compositional values calculated in this way are also given in Tables 7 and 8. In addition to the expected Y, Ti and O, the clusters were also enriched by Cr. The high levels of Cr associated with the nano-oxides that are observed in similar ODS steels have been attributed to a core–shell structure [56,58,60]. The presence of a Cr shell around the Y-Ti-O clusters was not clearly apparent in our studies, similar to previous APT observations for small Y-Ti-O clusters with radiuses below 2 nm [56,58].

Another way to avoid the trajectory aberration issue is to investigate the elemental ratios among Y, Ti, and O, which are considered the main constituents of these oxide particles. The results, in the form of the average Y:Ti:O fractions in the oxides, are shown in Fig. 13. These ratios are 2:3:5 in the Fe-12Cr-YWT and 2:2:5 in the Fe-14Cr-YWT. There are several known Y–Ti–O phases, with Y_2TiO_5 and $Y_2Ti_2O_7$ frequently reported by TEM studies of different ODS steels [61–67]. While the averaged Y:Ti:O ratio obtained from our APT data does not match known Y-Ti-O phases, our data does agree with previous APT studies suggesting nano-sized oxides are non-stoichiometric transition phases

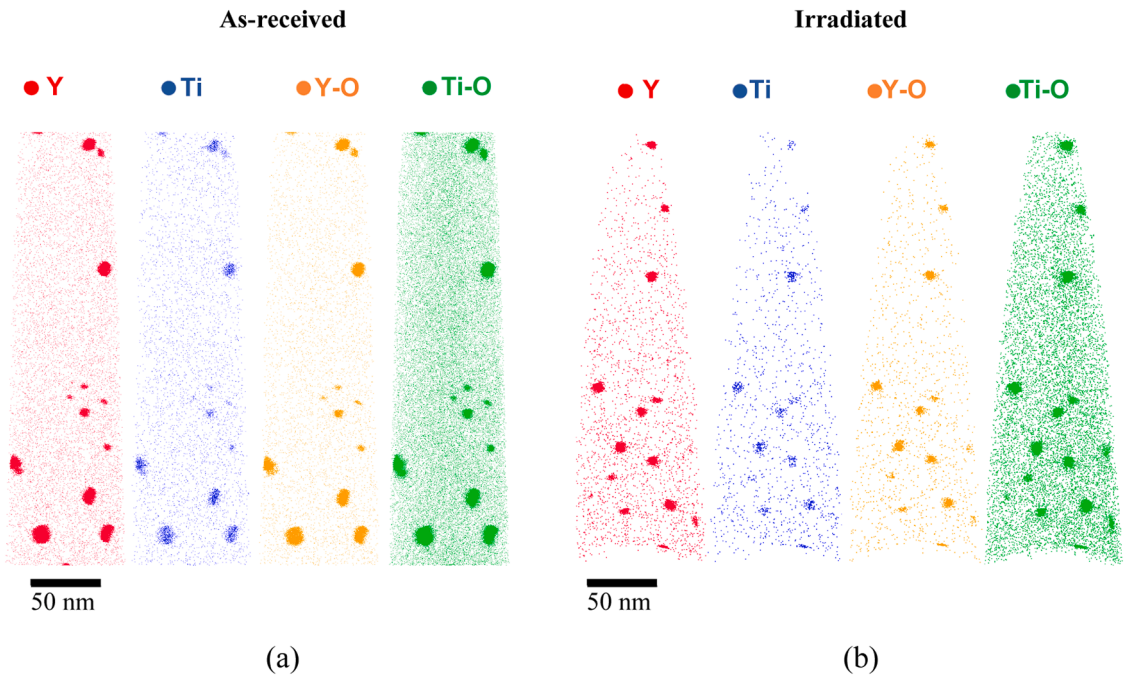

Fig. 10. Atom probe tomography reconstruction volumes (300×80×50 nm^3) of Fe–12Cr-YWT ODS steels before (a) and after (b) neutron irradiation in the HFR (3dpa, 600 °C). For clarity, only Y, T, Y-O and TiO ions are shown.

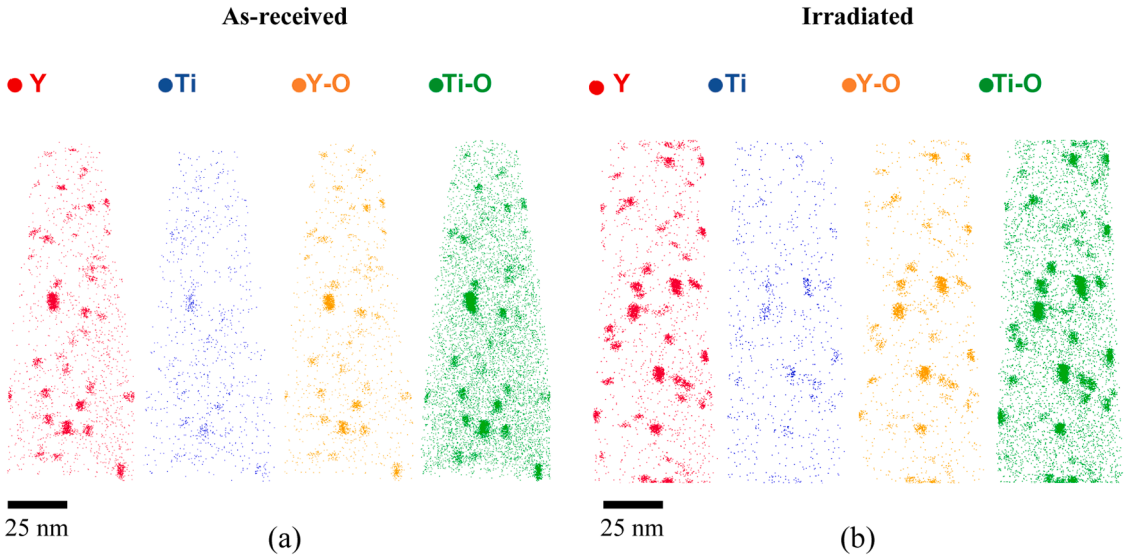

Fig. 11. Atom probe tomography reconstruction volumes (130×50×50 nm^3) of Fe–14Cr-YWT ODS steels before (a) and after (b) neutron irradiation in the HFR (3dpa, 600 °C). For clarity, only Y, T, Y-O and Ti-O ions are shown.

[29,68,69]. The data shows that all the main constituent elements inside Y-Ti-O particles remained almost unchanged during neutron irradiation, which agrees with the observed minor changes in the number density and sizes of the particles.

It also worth noting that our APT measurements showed 20 and 50 appm of Ar in Fe-12Cr-YWT and Fe-14Cr-YWT correspondently (Tables 4 and 5). Presence of this gas is known to originates from Ar trapping during mechanical alloying of ODS powder in an inert Ar atmosphere [26]. The APT data showed that the averaged matrix-corrected content of Ar in the ODS particles was up to 1500 appm (Table 7) suggesting strong tendency of this gas to agglomerate in the oxide particles.

4. Discussion

This study confirmed the excellent stability of ODS steels under high temperature neutron irradiation. The HFR irradiation at 600 °C led to very minor changes of the tensile properties of both Fe-12Cr-YWT and Fe-14Cr-YWT steels. Fig. 14 presents a summary of literature data on the yield stress (YS) behaviour of various ODS steels subjected to neutron irradiation within the temperature range of 500–670 °C [70–72]. In cases where YS data is unavailable, corresponding changes in ultimate tensile strength (UTS) or Vickers hardness (HV) are considered [73–75]. These data are evaluated alongside the results from our study. Notably, the mechanical strength of irradiated ODS steels generally remains within ±10 % of their non-irradiated counterparts, even at

Table 6
Number density and mean radius of the ODS precipitates steels before and after neutron irradiation in the HFR (3dpa, 600 °C), as measured by APT.

Element	Fe-12Cr-WTY		Fe-14Cr-WTY	
	Before irradiation (averaged over 223 clusters)	After irradiation (averaged over 66 clusters)	Before irradiation (averaged over 143 clusters)	After irradiation (averaged over 1410 clusters)
Average ND (m^{-3})	5.5×10^{22}	6.1×10^{22}	3.9×10^{23}	3.9×10^{23}
Min ND (m^{-3})	1.4×10^{22}	1.4×10^{22}	3.6×10^{23}	3.7×10^{23}
Max ND (m^{-3})	2.3×10^{23}	7.9×10^{22}	4.2×10^{23}	3.9×10^{23}
Average D, nm	2.5 ± 1.1	3.2 ± 2.2	2.2 ± 0.5	2.5 ± 0.7

exceptionally high doses exceeding 100 dpa. This trend largely agrees with our observations. However, an increase up to 25 % of YS has been observed previously for 14YWT-ODS specimens irradiated to 1.5 dpa in HFIR (ORNL, USA) at 580 and 670 °C and tensile tested in the range 500–600 °C [71]. At the same time no hardening was observed for the samples from the same irradiation but tensile tested at room temperature [71]. Also, almost 20 % hardening has been observed in the 11Cr-ODS (1DS) specimens irradiated to 17 dpa in the fast JOYO reactor (Japan) at 525 and 550 °C and tensile tested at irradiation temperatures [72]. At the same such increase was not observed in chemically similar the 12Cr-ODS (F94) and 12Cr-ODS (F95) steels irradiated and tested at similar conditions [72]. Links between chemistry, microstructural parameters of the ODS steels and the observed high temperature irradiation hardening behaviour remains unclear. These highlights the need for more irradiation experiments including exposure to much higher doses to further evaluate the irradiation resistance of ODS steels and inform the prediction of ODS steel behaviour in future fusion machines.

Minor changes in mechanical properties agrees with our detailed microstructural examination which showed the nanosized Y-Ti-O precipitates remain almost unaffected by exposure in the HFR. Both observations are in good agreement with the previously observed trends (see reviews [1,25,26]). Our experiments showed that at a microstructural level, extensive redistribution of tungsten appeared to be the most prominent change under high temperature exposure in the HFR. Indeed, APT and TEM measurements showed that about half of tungsten homogenously distributed in the Fe-Cr matrix of the steels before irradiation, diffused towards grain boundaries resulting in the formation of W-rich Laves phase during the HFR exposure.

Tungsten is added to Fe-Cr based steels for high-temperature applications to enhance creep rupture strength by improving solution hardening and stabilising $M_{23}C_6$ carbides [3]. It has also been observed to affect the yield strength and strain hardening [76] as well as microstructural processes controlled by vacancy diffusion, such as segregation and precipitation [77]. In this study, the change in tensile properties observed was minimal, suggesting that the microstructural evolution and redistribution of tungsten has not had a significant effect. This agrees with the analysis of Narita et al. [78] suggesting that 2 wt. % of dissolved tungsten in the 9Cr ODS may be responsible of only 18 MPa increase of the yield strength of the steel. However, it is expected that

Table 7
Compositions of the Y-Ti-O clusters in the Fe-12Cr-YWT before and after irradiation (3dpa, 600 °C) as measured by APT. In the as-received condition, data were averaged over 223 clusters, in the irradiated condition, the analysis was averaged over 66 clusters.

Element	Fe-12Cr-YWT			
	Y-Ti-O Raw concentration		Y-Ti-O Matrix-corrected	
	Before irradiation (at %)	After irradiation (at %)	Before irradiation (at %)	After irradiation (at %)
Y	4.4 ± 1.1	5.1 ± 1.3	11.6 ± 1.2	12.4 ± 1.2
Ti	7.04±2.4	8.2 ± 2.4	18.7 ± 3.7	19.9 ± 3.3
O	12.2 ± 3.4	14.3 ± 4.1	32.4 ± 4.6	34.8 ± 4.8
Cr	15.2 ± 1.6	14.4 ± 0.1	34.4 ± 9.1	30.4 ± 8.1
W	0.3 ± 0.1	0.2 ± 0.1	0.9 ± 0.4	0.6 ± 0.3
Mn	0.08±0.03	0.11±0.05	0.21±0.05	0.28±0.11
Si	0.19±0.07	0.27±0.11	0.49±0.12	0.65±0.41
C	0.07 ± 0.02	0.07 ± 0.01	0.19±0.03	0.18 ± 0.02
N	0.19±0.06	0.12±0.02	0.5 ± 0.3	0.3 ± 0.1
Ar	0.06±0.01	0.03±0.01	0.15±0.07	0.07±0.01
Fe	60.1 ± 5.3	57.1 ± 6.6	-	-

Table 8
Compositions of the Y-Ti-O clusters in the Fe-14Cr-YWT before and after irradiation (3dpa, 600 °C) as measured by APT. In the as-received condition, data were averaged over 143 clusters, in the irradiated condition, the analysis was averaged over 1410 clusters.

Element	Fe-14Cr-YWT			
	Y-Ti-O Raw concentration		Y-Ti-O Matrix-corrected	
	Before irradiation (at %)	After irradiation (at %)	Before irradiation (at %)	After irradiation (at %)
Y	2.8 ± 0.3	2.4 ± 0.3	8.9 ± 0.8	8.9 ± 0.4
Ti	3.3 ± 0.2	2.7 ± 0.4	10.5 ± 0.4	10.1 ± 0.7
O	6.9 ± 0.4	5.4 ± 0.8	21.9 ± 1.1	19.9 ± 1.5
Cr	21.2 ± 1.1	18.7 ± 0.6	55.4 ± 1.9	58.1 ± 2.4
W	0.5 ± 0.1	0.2 ± 0.1	1.6 ± 0.3	0.9 ± 0.1
Mn	0.03±0.01	0.03±0.01	0.09±0.03	0.12±0.02
Si	0.09±0.04	0.14±0.03	0.32±0.13	0.52±0.08
C	0.06 ± 0.04	0.02 ± 0.01	0.18±0.02	0.06 ± 0.01
N	0.26±0.06	0.23±0.05	0.82±0.2	0.85±0.22
Ar	0.02±0.01	0.01±0.01	0.07±0.01	0.05±0.01
Fe	64.7 ± 0.5	70.1 ± 2.1	-	-

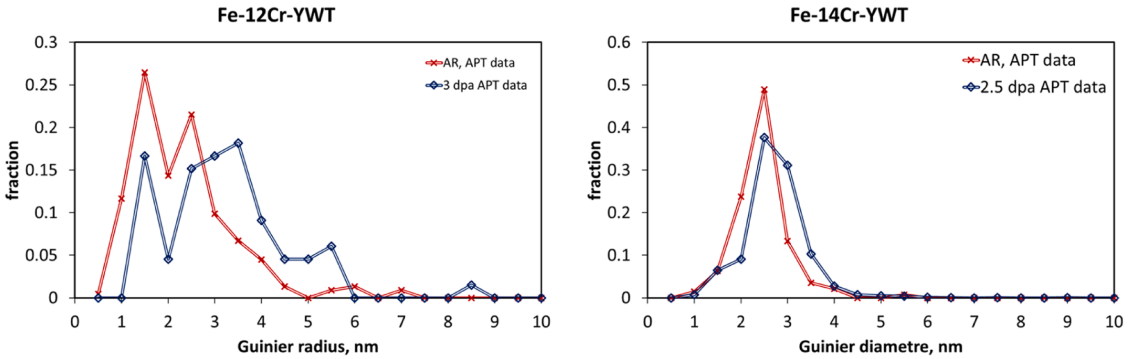

Fig. 12. Size (Guinier diameter) distribution of nanosized Y-Ti-O clusters distributed in the matrix before and after irradiation (3dpa, 600 °C).

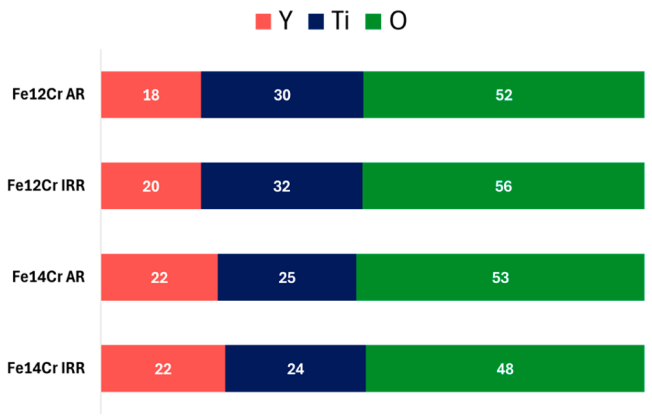

Fig. 13. Comparison of Y:Ti:O fractions in Y-Ti-O oxides in as-received and neutron irradiated (3dpa, 600 °C) Fe-12Cr-YWT and Fe-14Cr-YWT ODS steels.

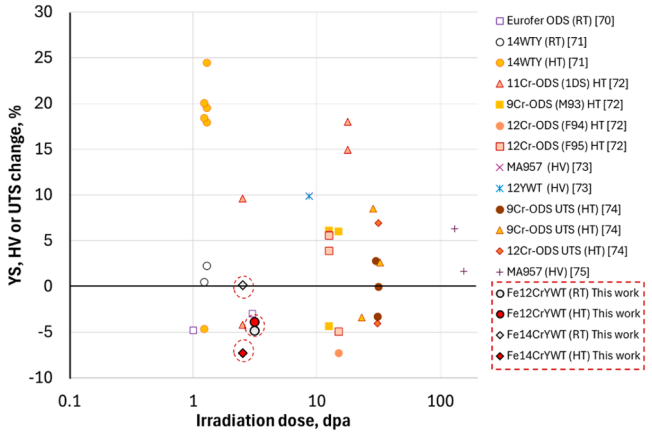

Fig. 14. Compilation of hardening behaviour in ODS alloys irradiated in various materials testing reactors (MTRs) within the temperature range of 500–670 °C [70–72]. Reported values primarily reflect changes in yield stress (YS), but where YS data is unavailable, changes in ultimate tensile strength (UTS) or Vickers hardness (HV) are provided as alternative indicators [73–75].

precipitation and growth of the Laves phase might lead to deterioration of fracture properties by increasing the ductile-to-brittle transition temperature and decreasing the upper shelf energy [3,79], although the exact mechanism has not been identified. This highlights the need for detailed experimental investigation into the effects of Laves phases on fracture properties of irradiated ODS steels.

To provide a comparison of the expected stability and fraction of Laves phase in alloys of these compositions, ThermoCalc 2024a was used to model the volume fraction, and matrix W composition after 180 days thermal ageing at 600 °C, shown in Fig. 15.

ThermoCalc equilibrium modelling suggested that the C14 Laves phase is thermodynamically stable in both alloys at temperatures below 700 °C, which is well above the maximum HFR irradiation temperature. The modelled Laves phase volume fraction (Table 9), after ageing for 180 days at 600 °C, is expected to be around 1.6 %, which agrees with the estimates determined from STEM images (Table 9). This suggests that the observed precipitation is thermodynamically driven and not neutron irradiation induced.

Previous investigations of neutron irradiated ODS steels at 560 °C, up to 21 dpa in the JOYO fast reactor, observed Laves phase forming in the high temperature specimens, and also concluded that this microstructural evolution was primarily thermally driven, not a radiation effect [50].

At the same time, ThermoCalc predicted that the W content in the

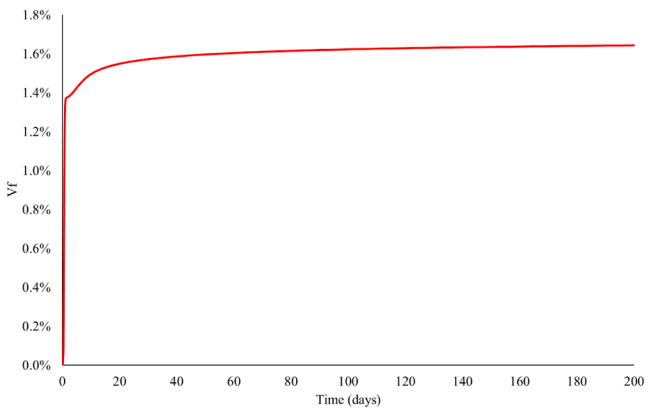

Fig. 15. vol fraction of Laves phase at grain boundaries, in Fe-12Cr ODS annealed at 600 °C, modelled using ThermoCalc2024a.

Table 9
ThermoCalc PRISMA predictions of Laves phase volume fraction and remaining tungsten content after ageing at 600 °C for 180 days, compared with TEM observed phase fraction in the neutron irradiated (3dpa, 600 °C) steels.

	ThermoCalc thermal ageing		STEM and APT data HFR irradiation	
	Volume fraction of Laves Phase, %	W matrix content, wt %	Area fraction of Laves Phase, %	W matrix content, wt %
Fe-12Cr-YWT	1.64	0.41	1.59 ± 0.08	0.83
Fe-14Cr-YWT	1.63	0.40	1.79 ± 0.03	0.89

matrix of both alloys was substantially lower than that measured by APT after neutron irradiation. That indicates the need for further investigation of Laves phase precipitation, including potential displacement damage effects. In general, the influence of tungsten on the performance of Fe-Cr based steels under irradiation is not well studied. Computational studies using first principles calculations have suggested that W exhibits a rather weak interaction with self-interstitial atoms in the bcc Fe matrix, but it shows strong binding with a vacancy and is capable of binding with several of them [77,80]. Therefore, W could play an important role in the processes controlled by vacancy diffusion, such as precipitation, segregation and swelling. For example, increased W content has been found to slow down helium bubble migration [81]. Also, Bonny et al. [80] concluded that W in Fe-Cr based alloys under irradiation suppress the nucleation of stable vacancy clusters, which otherwise may grow into voids.

It is worth emphasizing that we observed major redistribution of tungsten in both Fe-Cr ODS steels after relatively moderate 3 dpa neutron exposure during 208 full power days in the reactor. It is an order of magnitude lower that the exposure expected in future fusion power plants where the displacement damage dose above 20 dpa/year [82] and the total dose above 100 dpa after 5 years of operation are expected. Such fast redistribution of one of the major alloying elements highlights the fact that the optimisation of the W content in RAFM and ODS steels for fusion, and research towards the understanding of tungsten alloying effects under irradiation in Fe-Cr based steels, is still ongoing and requires more experimental data.

5. Conclusions

The microstructure and tensile properties of two HIPped Fe-12Cr-YWT and Fe-14Cr-YWT ODS steels were investigated before and after HFR neutron irradiation at a nominal temperature of 600 °C up to 3 dpa.

This study confirms high mechanical stability of ODS steels under neutron exposure at high temperatures. The irradiation resulted in very minor changes of the room temperature and high temperature tensile properties of both ODS steels, with a very small decrease in yield strength and ultimate tensile strength (<3 %) and almost unchanged plastic properties.

Before irradiation TEM showed fine distributions of nanometric Y-Ti-O (< 10 nm) in the matrix, larger Y-Ti-O (10–30 nm) oxides as well as TiO_2 based oxides (50–300 nm) oxides at grain boundaries. The morphology and number density of these clusters remained consistent after irradiation, although about 20 % increase in the average size of the nanometric Y-Ti-O oxides was observed by APT. A W-rich Laves phase precipitated on grain boundaries due to the elevated temperature of irradiation, leading to a significant 50 % reduction in W content in the matrix. In addition to this, a higher number density of Cr rich carbides was observed in the Fe-12Cr-YWT steel after irradiation.

Further work is currently ongoing to investigate the effect of higher dose irradiation on the oxide particles and alloying elements behaviour, to help determine the suitability of the material for fusion and next generation fission applications.

CRediT authorship contribution statement

Viacheslav Kuksenko: Writing – review & editing, Writing – original draft, Visualization, Supervision, Methodology, Investigation, Funding acquisition, Formal analysis, Data curation, Conceptualization. **Alexandra C. Dickinson-Lomas:** Writing – review & editing, Writing – original draft, Visualization, Investigation, Data curation. **Murthy Kolluri:** Writing – review & editing, Resources, Investigation. **Tjark van Staveren:** Writing – review & editing, Investigation, Data curation. **Amy S. Gandy:** Writing – review & editing, Supervision, Resources, Funding acquisition, Conceptualization.

Declaration of competing interest

The authors declare the following financial interests/personal relationships which may be considered as potential competing interests:

Viacheslav Kuksenko and Amy Gandy reports financial support was provided by Engineering and Physical Sciences Research Council. Murthy Kolluri and Tjark van Staveren reports financial support was provided by Dutch ministry of Economic Affairs and Climate. If there are other authors, they declare that they have no known competing financial interests or personal relationships that could have appeared to influence the work reported in this paper.

Acknowledgments

This work has been part-funded by the EPSRC Energy Programme [grant number EP/W006839/1]. The work presented in this paper has been performed as a part of NRG PALLAS's multi-annual PIONIER R&D program sponsored by the Dutch ministry of Economic Affairs and Climate.

The materials that were studied in this research were irradiated within the framework of the EXTREMAT IP project. This project has received funding from the Euratom research and training programme from 2004 to 2010 under grant agreement no. 500253. The contribution of partners in the EXTREMAT IP project is acknowledged.

We thank to Dr. Ed Pickering and Dr Elisabeth Francis (Henry Royce Institute, Electron Microscopy centre at the University of Manchester) for their support with the TEM studies.

Appendix A

Engineering tensile properties of Fe-12Cr-YWT and Fe-14Cr-YWT ODS steels irradiated at a target temperature of 600 °C to fluences ($E > 1$ MeV) of 2.16×1025m-2 (3.14 dpa) and 1.71×1025m-2 (2.51 dpa), respectively

	Test temperature (°C)	YS (MPa)	UTS, (MPa)	TE (%)	UE (%)
Fe-12Cr-YWT as-received	24	745	940	14.5	9.5
	150	631	807	12.8	8.2
	300	608	768	12.1	8.3
	400	577	715	10.7	5.9
	500	479	596	16.8	6.3
	550	419	510	20.8	9
	550	423	495	20.2	9.2
	600	415	475	19.1	2.9
Fe-12Cr-YWT irradiated (3.14 dpa, 600 °C)	24	709	915	15.0	10.1
	150	637	814	13.2	8.8
	300	576	736	13.0	8.2
	400	542	681	13.8	7.9
	500	476	578	17.3	7.4
	550	418	492	17.4	9.4
	600	399	459	19.0	5.1
	Test temperature (°C)	YS (MPa)	UTS, (MPa)	TE (%)	UE (%)
Fe-14Cr-YWT irradiated	24	743	920	11.5	6.7
	150	695	848	11.7	7.4
	300	635	772	8.7	5.2
	400	632	753	7.9	4.9
	500	527	617	11.4	4.3
	550	457	537	14.3	6.5
	600	440	501	13	4.1
Fe-14Cr-YWT irradiated (2.51 dpa, 600 °C)	24	744	948.0	12.5	7.4
	150	685	841.0	7.5	6.2
	300	650	778.0	8.1	4.8
	400	578	695.0	9.9	5.7
	500	507	598.0	9.2	5.1

(*continued on next page*)

(*continued*)

	Test temperature (°C)	YS (MPa)	UTS, (MPa)	TE (%)	UE (%)
	550	447	516.0	13.2	7.6
	600	408	461.0	12.7	1.9

Data availability

Data will be made available on request.

References

[1] R.L. Klueh, D.R. Harries, High-Chromium Ferritic and Martensitic Steels For Nuclear Applications, ASTM, 2001.

[2] L. Tan, Y. Katoh, L.L. Snead, Development of castable nanostructured alloys as a new generation RAFM steels, J. Nucl. Mater. 511 (2018) 598–604, https://doi.org/10.1016/j.jnucmat.2018.05.024.

[3] F. Abe, T.-U. Kern, R. Viswanathan, Creep-Resistant Steels, Elsevier, 2008.

[4] S.J. Zinkle, Advanced materials for fusion technology, Fusion Eng. Des. 74 (2005) 31–40, https://doi.org/10.1016/j.fusengdes.2005.08.008.

[5] N. Baluc, J.L. Boutard, S.L. Dudarev, M. Rieth, J.B. Correia, B. Fournier, J. Henry, F. Legendre, T. Leguey, M. Lewandowska, R. Lindau, E. Marquis, A. Muñoz, B. Radiguet, Z. Oksiuta, Review on the EFDA work programme on nano-structured ODS RAF steels, J. Nucl. Mater. 417 (2011) 149–153, https://doi.org/10.1016/j.jnucmat.2010.12.065.

[6] C. Fazio, A. Alamo, A. Almazouzi, S. De Grandis, D. Gomez-Briceno, J. Henry, L. Malerba, M. Rieth, European cross-cutting research on structural materials for Generation IV and transmutation systems, J. Nucl. Mater. 392 (2009) 316–323, https://doi.org/10.1016/j.jnucmat.2009.03.020.

[7] Y. de Carlan, J.-L. Bechade, P. Dubuisson, J.-L. Seran, P. Billot, A. Bougault, T. Cozzika, S. Doriot, D. Hamon, J. Henry, M. Ratti, N. Lochet, D. Nunes, P. Olier, T. Leblond, M.H. Mathon, CEA developments of new ferritic ODS alloys for nuclear applications, J. Nucl. Mater. 386–388 (2009) 430–432, https://doi.org/10.1016/j.jnucmat.2008.12.156.

[8] S.J. Zinkle, G.S. Was, Materials challenges in nuclear energy, Acta Mater. 61 (2013) 735–758, https://doi.org/10.1016/j.actamat.2012.11.004.

[9] S. Ukai, M. Harada, H. Okada, M. Inoue, S. Nomura, S. Shikakura, K. Asabe, T. Nishida, M. Fujiwara, Alloying design of oxide dispersion strengthened ferritic steel for long life FBRs core materials, J. Nucl. Mater. 204 (1993) 65–73, https://doi.org/10.1016/0022-3115(93)90200-I.

[10] S. Ukai, M. Fujiwara, Perspective of ODS alloys application in nuclear environments, J. Nucl. Mater. 307–311 (2002) 749–757, https://doi.org/10.1016/S0022-3115(02)01043-7.

[11] P. Dubuisson, Y. de Carlan, V. Garat, M. Blat, ODS ferritic/martensitic alloys for Sodium Fast Reactor fuel pin cladding, J. Nucl. Mater. 428 (2012) 6–12, https://doi.org/10.1016/j.jnucmat.2011.10.037.

[12] G.R. Odette, M.J. Alinger, B.D. Wirth, Recent developments in irradiation-resistant steels, Annu. Rev. Mater. Res. 38 (2008) 471–503, https://doi.org/10.1146/annurev.matsci.38.060407.130315.

[13] E. Materna-Morris, R. Lindau, H.-C. Schneider, A. Möslang, Tensile behavior of EUROFER ODS steel after neutron irradiation up to 16.3 dpa between 250 and 450°C, Fusion Eng. Des. 98–99 (2015) 2038–2041, https://doi.org/10.1016/j.fusengdes.2015.07.015.

[14] N. Hashimoto, R. Kasada, B. Raj, M. Vijayalakshmi, 3.05 - Radiation effects in ferritic steels and advanced ferritic-martensitic steels☆, in: R.J.M. Konings, R. E. Stoller (Eds.), Comprehensive Nuclear Materials, 2nd ed., Elsevier, Oxford, 2020, pp. 226–254, https://doi.org/10.1016/B978-0-12-803581-8.12051-X.

[15] E.A. Little, L.P. Stoter, Microstructural stability of fast reactor irradiated 10–12%Cr ferritic-martensitic stainless steels, ASTM-STP 782 (1982) 207.

[16] P.J. Maziasz, R.L. Klueh, J.M. Vitek, Helium effects on void formation in 9Cr-1MoVNb and 12Cr-1MoVW irradiated in HFIR, J. Nucl. Mater. 141–143 (Part 2) (1986) 929–937, https://doi.org/10.1016/0022-3115(86)90120-0.

[17] P. Dubuisson, D. Gilbon, J.L. Séran, Microstructural evolution of ferritic-martensitic steels irradiated in the fast breeder reactor Phénix, J. Nucl. Mater. 205 (1993) 178–189, https://doi.org/10.1016/0022-3115(93)90080-I.

[18] A.M. Dvoriashin, S.I. Porollo, Yu.V. Konobeev, F.A. Garner, Influence of high dose neutron irradiation on microstructure of EP-450 ferritic–martensitic steel irradiated in three Russian fast reactors, J. Nucl. Mater. 329–333 (Part A) (2004) 319–323, https://doi.org/10.1016/j.jnucmat.2004.04.309.

[19] S.I. Porollo, A.M. Dvoriashin, Yu.V. Konobeev, F.A. Garner, Microstructure and mechanical properties of ferritic/martensitic steel EP-823 after neutron irradiation to high doses in BOR-60, J. Nucl. Mater. 329–333 (Part A) (2004) 314–318, https://doi.org/10.1016/j.jnucmat.2004.04.310.

[20] B.H. Sencer, J.R. Kennedy, J.I. Cole, S.A. Maloy, F.A. Garner, Microstructural analysis of an HT9 fuel assembly duct irradiated in FFTF to 155 dpa at 443°C, J. Nucl. Mater. 393 (2009) 235–241, https://doi.org/10.1016/j.jnucmat.2009.06.010.

[21] J.J. Kai, R.L. Klueh, Microstructural analysis of neutron-irradiated martensitic steels, J. Nucl. Mater. 230 (1996) 116–123, https://doi.org/10.1016/0022-3115(96)00165-1.

[22] T.S. Morgan, E.A. Little, R.G. Faulner, Microstructural studies in fast reactor irradiated FV448 ferritic-martensitic alloy plate and weldment, effect of radiation on materials, in: R.E. Stoller, A.S. Kumar, D.S. Gelles (Eds.), Proceedings of the 16th International Symposium, ASTM, 1994, p. 607. STP 1175.

[23] Y. Kohno, D.S. Gelles, A. Kohyama, M. Tamura, A. Hishinuma, Irradiation response of a reduced activation Fe-8Cr-2W martensitic steel (F82H) after FFTF irradiation, J. Nucl. Mater. 191–194 (Part B) (1992) 868–873, https://doi.org/10.1016/0022-3115(92)90597-E.

[24] Y. Kohno, A. Kohyama, M. Yoshino, K. Asakura, Effects of neutron irradiation on microstructural evolution in candidate low activation ferritic steels, J. Nucl. Mater. 212–215 (Part 1) (1994) 707–713, https://doi.org/10.1016/0022-3115(94)90149-X.

[25] J.P. Wharry, M.J. Swenson, K.H. Yano, A review of the irradiation evolution of dispersed oxide nanoparticles in the b.c.c. Fe-Cr system: current understanding and future directions, J. Nucl. Mater. 486 (2017) 11–20, https://doi.org/10.1016/j.jnucmat.2017.01.009.

[26] S. Ukai, N. Oono-Hori, S. Ohtsuka, 3.06 - Oxide dispersion strengthened steels☆ (Eds.), in: R.J.M. Konings, R.E. Stoller (Eds.), Comprehensive Nuclear Materials, 2nd ed., Elsevier, Oxford, 2020, pp. 255–292, https://doi.org/10.1016/B978-0-12-803581-8.11718-7.

[27] J.G. van der Laan, J.B.J. Hegeman, J.A. Vreeling, O. Wouters, D.E. Buckthorpe, M. W. Davies, H.H. Bolt, The European irradiation Test program at HFR Petten to support materials development and qualification of helium cooled reactor components, in: South Africa, 2006.

[28] Z. Oksiuta, N. Baluc, Optimization of the chemical composition and manufacturing route for ODS RAF steels for fusion reactor application, Nucl. Fusion 49 (2009) 055003, https://doi.org/10.1088/0029-5515/49/5/055003.

[29] P. Unifantowicz, T. Płociński, C.A. Williams, R. Schäublin, N. Baluc, Structure of complex oxide nanoparticles in a Fe–14Cr–2W–0.3Ti–0.3Y2O3 ODS RAF steel, J. Nucl. Mater. 442 (2013) S158–S163, https://doi.org/10.1016/j.jnucmat.2013.04.048.

[30] P. Olier, Z. Oksiuta, J.F. Melat, D. Hamon, T. Leblond, Y. de Carlan, N.L. Baluc, Microstructural and cold workability assessment of a new ODS ferritic steel, Adv. Mater. Res. 59 (2009) 313–318, https://doi.org/10.4028/www.scientific.net/AMR.59.313.

[31] T.O. van Staveren, EXTREMAT PIE results ODS steel (EFDA meeting), (2011).

[32] ASTM E8/E8M-22. Standard test methods for tension testing of metallic materials, (2024). 10.1520/E0008_E0008M-22.

[33] Standard practice for determining average grain size using electron backscatter diffraction (EBSD) in fully recrystallized polycrystalline materials, (n.d.). https://www.astm.org/e2627-13r19.html (accessed January 21, 2025).

[34] F. de la Peña, E. Prestat, J. Lähnemann, V.T. Fauske, P. Burdet, P. Jokubauskas, T. Furnival, C. Francis, M. Nord, T. Ostasevicius, K.E. MacArthur, D.N. Johnstone, M. Sarahan, J. Taillon, T. Aarholt, pquinn-dls, V. Migunov, A. Eljarrat, J. Caron, T. Nemoto, T. Poon, S. Mazzucco, actions-user, sivborg, N. Tappy, N. Cautaerts, S. Somnath, T. Slater, M. Walls, pietsjoh, hyperspy/hyperspy: v2.2.0, (2024). 10.5281/zenodo.14057415.

[35] J. Schindelin, I. Arganda-Carreras, E. Frise, V. Kaynig, M. Longair, T. Pietzsch, S. Preibisch, C. Rueden, S. Saalfeld, B. Schmid, J.-Y. Tinevez, D.J. White, V. Hartenstein, K. Eliceiri, P. Tomancak, A. Cardona, Fiji: an open-source platform for biological-image analysis, Nat. Methods 9 (2012) 676–682, https://doi.org/10.1038/nmeth.2019.

[36] M.K. Miller, Atom Probe Tomography: Analysis at the Atomic Level, Kluwer Academic/Plenum Publishers, New York, 2000.

[37] B. Gault, M.P. Moody, J.M. Cairney, S.P. Ringer, Atom Probe Microscopy, Springer Series in Materials Science, 2012.

[38] C.A. Williams, D. Haley, E.A. Marquis, G.D.W. Smith, M.P. Moody, Defining clusters in APT reconstructions of ODS steels, Ultramicroscopy 132 (2013) 271–278, https://doi.org/10.1016/j.ultramic.2012.12.011.

[39] J.-O. Andersson, T. Helander, L. Höglund, P. Shi, B. Sundman, Thermo-Calc & DICTRA, computational tools for materials science, CALPHAD 26 (2002) 273–312, https://doi.org/10.1016/S0364-5916(02)00037-8.

[40] D.T. Hoelzer, J. Bentley, M.A. Sokolov, M.K. Miller, G.R. Odette, M.J. Alinger, Influence of particle dispersions on the high-temperature strength of ferritic alloys, J. Nucl. Mater. 367–370 (2007) 166–172, https://doi.org/10.1016/j.jnucmat.2007.03.151.

[41] D.A. McClintock, M.A. Sokolov, D.T. Hoelzer, R.K. Nanstad, Mechanical properties of irradiated ODS-EUROFER and nanocluster strengthened 14YWT, J. Nucl. Mater. 392 (2009) 353–359, https://doi.org/10.1016/j.jnucmat.2009.03.024.

[42] J. Macías-Delgado, T. Leguey, V. de Castro, M.A. Auger, M.A. Monge, P. Spätig, N. Baluc, R. Pareja, Microstructure and tensile properties of ODS ferritic steels

mechanically alloyed with Fe2Y, Nucl. Mater. Energy 9 (2016) 372–377, https://doi.org/10.1016/j.nme.2016.09.019.
[43] H. Kishimoto, M.J. Alinger, G.R. Odette, T. Yamamoto, TEM examination of microstructural evolution during processing of 14CrYWTi nanostructured ferritic alloys, J. Nucl. Mater. 329–333 (2004) 369–371, https://doi.org/10.1016/j.jnucmat.2004.04.044.
[44] P. He, M. Klimenkov, R. Lindau, A. Möslang, Characterization of precipitates in nano structured 14% Cr ODS alloys for fusion application, J. Nucl. Mater. 428 (2012) 131–138, https://doi.org/10.1016/j.jnucmat.2011.08.026.
[45] P. Miao, G.R. Odette, T. Yamamoto, M. Alinger, D. Hoelzer, D. Gragg, Effects of consolidation temperature, strength and microstructure on fracture toughness of nanostructured ferritic alloys, J. Nucl. Mater. 367–370 (2007) 208–212, https://doi.org/10.1016/j.jnucmat.2007.03.144.
[46] Ch.Ch. Eiselt, M. Klimenkov, R. Lindau, A. Möslang, H.R.Z. Sandim, A.F. Padilha, D. Raabe, High-resolution transmission electron microscopy and electron backscatter diffraction in nanoscaled ferritic and ferritic–martensitic oxide dispersion strengthened–steels, J. Nucl. Mater. 385 (2009) 231–235, https://doi.org/10.1016/j.jnucmat.2008.11.029.
[47] G. Spartacus, J. Malaplate, D. Menut, C. Toffolon-Masclet, D. Sornin, R. Guillou, A. Gangloff, S. Urvoy, F. De Geuser, A. Deschamps, Characterization of the nature and morphology of coarse precipitation in various oxide dispersion strengthened steels, Materialia 17 (2021) 101117, https://doi.org/10.1016/j.mtla.2021.101117 (Oxf).
[48] M.K. Miller, D.T. Hoelzer, Effect of neutron irradiation on nanoclusters in MA957 ferritic alloys, J. Nucl. Mater. 418 (2011) 307–310, https://doi.org/10.1016/j.jnucmat.2011.07.031.
[49] A. Bhattacharya, S.J. Zinkle, J. Henry, S.M. Levine, P.D. Edmondson, M.R. Gilbert, H. Tanigawa, C.E. Kessel, Irradiation damage concurrent challenges with RAFM and ODS steels for fusion reactor first-wall/blanket: a review, J. Phys. Energy 4 (2022) 034003, https://doi.org/10.1088/2515-7655/ac6f7f.
[50] S. Yamashita, K. Oka, S. Ohnuki, N. Akasaka, S. Ukai, Phase stability of oxide dispersion-strengthened ferritic steels in neutron irradiation, J. Nucl. Mater. 307–311 (2002) 283–288, https://doi.org/10.1016/S0022-3115(02)01077-2.
[51] S. Yin, L. Yang, Y. Liu, R. Yang, Y. Wang, F. Zhao, Stabilities of the precipitates in CLAM steel during 30,000 h thermal aging, J. Nucl. Mater. 567 (2022) 153805, https://doi.org/10.1016/j.jnucmat.2022.153805.
[52] M. Oñoro, V. de Castro, T. Leguey, J. Pöpperlová, R.M. Huizenga, M.A. Auger, Microstructural stability of secondary phases in an ODS ferritic steel after thermal aging at 873 K, Mater. Charact. 207 (2024) 113517, https://doi.org/10.1016/j.matchar.2023.113517.
[53] M. Oñoro, J. Macías-Delgado, M.A. Auger, V. de Castro, T. Leguey, Mechanical properties and stability of precipitates of an ODS steel after thermal cycling and aging, Nucl. Mater. Energy 24 (2020) 100758, https://doi.org/10.1016/j.nme.2020.100758.
[54] M. Oñoro, S.R. Parnell, E. Salas-Colera, D. Alba Venero, V. Martin-Diaconesu, T. Leguey, V. de Castro, M.A. Auger, Secondary phases characterization by SANS and XAS of an ODS ferritic steel after thermal aging at 873 K, Nucl. Mater. Energy 39 (2024) 101671, https://doi.org/10.1016/j.nme.2024.101671.
[55] A.L. Rouffié, J. Crépin, M. Sennour, B. Tanguy, A. Pineau, D. Hamon, P. Wident, S. Vincent, V. Garat, B. Fournier, Effect of the thermal ageing on the tensile and impact properties of a 18%Cr ODS ferritic steel, J. Nucl. Mater. 445 (2014) 37–42, https://doi.org/10.1016/j.jnucmat.2013.10.030.
[56] C.A. Williams, E.A. Marquis, A. Cerezo, G.D.W. Smith, Nanoscale characterisation of ODS–Eurofer 97 steel: an atom-probe tomography study, J. Nucl. Mater. 400 (2010) 37–45, https://doi.org/10.1016/j.jnucmat.2010.02.007.
[57] D.J. Larson, P.J. Maziasz, I.-S. Kim, K. Miyahara, Three-dimensional atom probe observation of nanoscale titanium-oxygen clustering in an oxide-dispersion-strengthened Fe-12Cr-3W-0.4Ti + Y2O3 ferritic alloy, Scr. Mater. 44 (2001) 359–364, https://doi.org/10.1016/S1359-6462(00)00593-5.
[58] A.J. London, S. Lozano-Perez, M.P. Moody, S. Amirthapandian, B.K. Panigrahi, C. S. Sundar, C.R.M. Grovenor, Quantification of oxide particle composition in model oxide dispersion strengthened steel alloys, Ultramicroscopy 159 (2015) 360–367, https://doi.org/10.1016/j.ultramic.2015.02.013.
[59] M.K. Miller, A. Cerezo, M.G. Hetherington and G.D.W. Smith., Atom probe field ion microscopy, Clarendon, Oxford, 1996.
[60] E.A. Marquis, Core/shell structures of oxygen-rich nanofeatures in oxide-dispersion strengthened Fe–Cr alloys, Appl. Phys. Lett. 93 (2008) 181904, https://doi.org/10.1063/1.3000965.
[61] S. Ukai, T. Okuda, M. Fujiwara, T. Kobayashi, S. Mizuta, H. Nakashima, Characterization of high temperature creep properties in recrystallized 12Cr-ODS ferritic steel claddings, J. Nucl. Sci. Technol. 39 (2002) 872–879, https://doi.org/10.1080/18811248.2002.9715271.
[62] M. Klimiankou, R. Lindau, A. Möslang, TEM characterization of structure and composition of nanosized ODS particles in reduced activation ferritic–martensitic steels, J. Nucl. Mater. 329–333 (2004) 347–351, https://doi.org/10.1016/j.jnucmat.2004.04.083.
[63] I.-S. Kim, J.D. Hunn, N. Hashimoto, D.L. Larson, P.J. Maziasz, K. Miyahara, E. H. Lee, Defect and void evolution in oxide dispersion strengthened ferritic steels under 3.2 MeV Fe+ ion irradiation with simultaneous helium injection, J. Nucl. Mater. 280 (2000) 264–274, https://doi.org/10.1016/S0022-3115(00)00066-0.
[64] T. Okuda, M. Fujiwara, Dispersion behaviour of oxide particles in mechanically alloyed ODS steel, J. Mater. Sci. Lett. 14 (1995) 1600–1603, https://doi.org/10.1007/BF00455428.
[65] Y. Wu, E.M. Haney, N.J. Cunningham, G.R. Odette, Transmission electron microscopy characterization of the nanofeatures in nanostructured ferritic alloy MA957, Acta Mater. 60 (2012) 3456–3468, https://doi.org/10.1016/j.actamat.2012.03.012.
[66] A.J. London, S. Lozano-Perez, S. Santra, S. Amirthapandian, B.K. Panigrahi, C. S. Sundar, C.R.M. Grovenor, Comparison of atom probe tomography and transmission electron microscopy analysis of oxide dispersion strengthened steels, J. Phys. Conf. Ser. 522 (2014) 012028, https://doi.org/10.1088/1742-6596/522/1/012028.
[67] H. Sakasegawa, L. Chaffron, F. Legendre, L. Boulanger, T. Cozzika, M. Brocq, Y. de Carlan, Correlation between chemical composition and size of very small oxide particles in the MA957 ODS ferritic alloy, J. Nucl. Mater. 384 (2009) 115–118, https://doi.org/10.1016/j.jnucmat.2008.11.001.
[68] M.K. Miller, E.A. Kenik, K.F. Russell, L. Heatherly, D.T. Hoelzer, P.J. Maziasz, Atom probe tomography of nanoscale particles in ODS ferritic alloys, Mater. Sci. Eng. A 353 (2003) 140–145, https://doi.org/10.1016/S0921-5093(02)00680-9.
[69] M.K. Miller, D.T. Hoelzer, E.A. Kenik, K.F. Russell, Nanometer scale precipitation in ferritic MA/ODS alloy MA957, J. Nucl. Mater. 329–333 (2004) 338–341, https://doi.org/10.1016/j.jnucmat.2004.04.085.
[70] N.V. Luzginova, H.S. Nolles, P. ten Pierick, T. Bakker, R.K. Mutnuru, M. Jong, D. T. Blagoeva, Irradiation response of ODS Eurofer97 steel, J. Nucl. Mater. 428 (2012) 192–196, https://doi.org/10.1016/j.jnucmat.2011.08.030.
[71] R.K. Nanstad, D.A. McClintock, D.T. Hoelzer, L. Tan, T.R. Allen, High temperature irradiation effects in selected generation IV structural alloys, J. Nucl. Mater. 392 (2009) 331–340, https://doi.org/10.1016/j.jnucmat.2009.03.022.
[72] S. Yamashita, T. Yoshitake, N. Akasaka, S. Ukai, A. Kimura, Mechanical behavior of oxide dispersion strengthened steels irradiated in JOYO, Mater. Trans. 46 (2005) 493–497, https://doi.org/10.2320/matertrans.46.493.
[73] A. Bhattacharya, J. Reed, X. Chen, J.W. Geringer, Y. Katoh, T. Nozawa, H. Tanigawa, Neutron Irradiation Induced Hardening in RAFM and ODS Steels. Fusion Materials Semi-Annual Progress Report for the Period Ending, 37831, Oak Ridge National Laboratory, Oak Ridge, Tennessee, 2021. https://www.ornl.gov/file/fusion-material-semiannual-report-december-2020/display.
[74] Y. Yano, R. Ogawa, S. Yamashita, S. Ohtsuka, T. Kaito, N. Akasaka, M. Inoue, T. Yoshitake, K. Tanaka, Effects of neutron irradiation on tensile properties of oxide dispersion strengthened (ODS) steel claddings, J. Nucl. Mater. 419 (2011) 305–309, https://doi.org/10.1016/j.jnucmat.2011.05.026.
[75] T. Toyama, T. Tanno, Y. Yano, K. Inoue, Y. Nagai, S. Ohtsuka, T. Miyazawa, M. Mitsuhara, H. Nakashima, M. Ohnuma, T. Kaito, Oxide particles in oxide dispersion strengthened steel neutron-irradiated up to 158 dpa at Joyo, J. Nucl. Mater. 599 (2024) 155252, https://doi.org/10.1016/j.jnucmat.2024.155252.
[76] J. Vanaja, K. Laha, M. Nandagopal, S. Sam, M.D. Mathew, T. Jayakumar, E. R Kumar, Effect of tungsten on tensile properties and flow behaviour of RAFM steel, J. Nucl. Mater. 433 (2013) 412–418, https://doi.org/10.1016/j.jnucmat.2012.10.040.
[77] G. Bonny, N. Castin, C. Domain, P. Olsson, B. Verreyken, M.I. Pascuet, D. Terentyev, Density functional theory-based cluster expansion to simulate thermal annealing in FeCrW alloys, Philos. Mag. 97 (2017) 299–317, https://doi.org/10.1080/14786435.2016.1258123.
[78] T. Narita, S. Ukai, S. Ohtsuka, M. Inoue, Effect of tungsten addition on microstructure and high temperature strength of 9CrODS ferritic steel, J. Nucl. Mater. 417 (2011) 158–161, https://doi.org/10.1016/j.jnucmat.2011.01.060.
[79] F. Abe, H. Araki, T. Noda, M. Okada, Microstructure and toughness of Cr-W and Cr-V ferritic steels, J. Nucl. Mater. 155–157 (1988) 656–661, https://doi.org/10.1016/0022-3115(88)90390-X.
[80] G. Bonny, N. Castin, J. Bullens, A. Bakaev, T.C.P. Klaver, D. Terentyev, On the mobility of vacancy clusters in reduced activation steels: an atomistic study in the Fe–Cr–W model alloy, J. Phys. Condens. Matter 25 (2013) 315401, https://doi.org/10.1088/0953-8984/25/31/315401.
[81] K. Ono, H. Sasagawa, F. Kudo, M. Miyamoto, Y. Hidaka, Effects of tungsten on thermal desorption of helium from Fe–9Cr–2W ferritic alloy irradiated with low energy helium ions, J. Nucl. Mater. 417 (2011) 1026–1029, https://doi.org/10.1016/j.jnucmat.2011.01.090.
[82] S.J. Zinkle, A. Möslang, Evaluation of irradiation facility options for fusion materials research and development, Fusion Eng. Des. 88 (2013) 472–482, https://doi.org/10.1016/j.fusengdes.2013.02.081.